JOURNAL OF GUIDANCE, CONTROL, AND DYNAMICS
Vol. 30, No. 2, March–April 2007

Cable Control of an Aerostat Platform: Experimental Results and Model Validation

Casey Lambert* and Meyer Nahon†
McGill University, Montreal, Quebec H3A 2K6, Canada
Dean Chalmers‡
Dominion Radio Astrophysical Observatory, Penticton, British Columbia V2A 6J9, Canada
and
Gabriele Gilardi§
University of Victoria, Victoria, British Columbia V8W 2Y2, Canada

DOI: 10.2514/1.22598

An aerial positioning system consisting of a helium-filled aerostat and three actuated tethers arranged in a tripod is studied. The original concept for the positioning system was introduced as part of a novel large-scale radio telescope. A one-third scale experimental system was developed to compare the dynamic response with the results given by a comprehensive nonlinear dynamics model developed previously. Flight tests were performed in the spring of 2005 that used position feedback and a proportional, integral, and derivative controller to demonstrate the disturbance rejection capabilities of the system. In this paper, the test results are compared with simulation results of the nonlinear model and good agreement was observed. Open-loop frequency response of the experimental system was also compared with that of a linear dynamics model, which also provided a good match. With the dynamics model validated, it was used as a design tool to investigate how certain system parameters, such as the number of tethers, affect performance.

Nomenclature

e_i	=	position error of payload in the ith tether direction
k_i	=	stiffness of the ith tether
K_D	=	derivative control gain
K_I	=	integral control gain
K_P	=	proportional control gain
L_i	=	length of the ith tether
R	=	focal length of a radio telescope
R_B	=	radius of the winch placement circle
$\boldsymbol{r}$	=	actual position of the payload
$\boldsymbol{r}_d$	=	desired position of the payload
$\boldsymbol{r}_{Wi}$	=	position of the ith winch
T_i	=	tension in the ith tether
U	=	mean wind speed
v_i	=	commanded velocity of the ith tether
$\boldsymbol{w}$	=	wind disturbance force
x	=	payload position in the x direction
y	=	payload position in the y direction
z	=	payload position in the z direction
ζ	=	damping ratio of winch actuator
θ_{az}	=	azimuth angle of receiver position for a radio telescope
θ_w	=	direction of the prevailing wind vector
θ_{ze}	=	angle between the zenith and the receiver position vector for a radio telescope
ω_n	=	natural frequency of the winch actuator

Received 20 January 2006; revision received 3 August 2006; accepted for publication 12 September 2006.

*Doctoral Candidate, Department of Mechanical Engineering, Room 351, 817 Sherbrooke Street West. Student Member AIAA.
†Associate Professor, Department of Mechanical Engineering, Room 351, 817 Sherbrooke Street West. Associate Fellow AIAA.
‡Research Engineer, P.O. Box 248.
§Research Assistant, Department of Mechanical Engineering, Room 548, 3800 Finnerty Road.

I. Introduction

AN aerial positioning system can be achieved using a lighter-than-air lifting body, or aerostat, attached to a series of actuated tethers anchored to the ground. One application that calls for such a positioning system is the proposed large adaptive reflector (LAR) radio telescope [1] shown in Fig. 1. This telescope concept is based on a large 200-m reflector composed of individually actuated panels supported by the ground. The panels form a shallow adaptive paraboloid, which has a focal length of 500 m. During operation, the antenna/feed package housed at the focal point must be positioned at points on a hemisphere down to a zenith angle of 60 deg, as shown in Fig. 2. The tracking of the desired position and a certain level of disturbance rejection can be realized by actively adjusting the lengths of the ground tethers using winches operating under closed-loop control.

Early investigations into the *passive* behavior of a multitethered aerostat system exposed to atmospheric conditions were conducted by the U.S. Air Force in 1973 [2]. They performed flight tests with an instrumented "natural-shaped" aerostat and demonstrated that when the payload was connected to three tethers in a tripod arrangement, it experienced much smaller displacements than with a single tether. They also found that separating the payload and the aerostat using a single tether or leash decreased the displacements further. A similar tritethered arrangement performed favorably when tested by Russian meteorologists [3], although this work did not include quantitative results.

The proposed multitethered aerostat positioning system is similar to the class of cable-driven parallel robot manipulators that has recently emerged following the development of Robocrane in the early 1990s [4]. Typical cable manipulators differ from the tethered aerostat system, because they rely on gravity as opposed to buoyancy to tension the tethers. Significant research has been conducted into the kinematics, dynamics, and control of cable manipulators [5–8], however, the size of their workspace is generally limited to several meters, which is about two orders of magnitude smaller than our tethered system. Because of the drastic difference in the lengths of the cables, which are the primary actuators, the modeling and experimental analysis techniques of the smaller parallel mechanisms do not include the important cable dynamics that affect the much larger aerial positioning system (perhaps the world's largest robotic

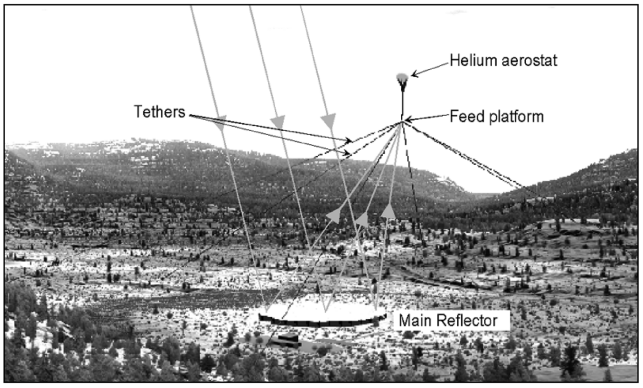

Fig. 1 Artist's concept of the LAR radio telescope concept featuring a panel-actuated reflector and a tethered aerostat feed positioning system.

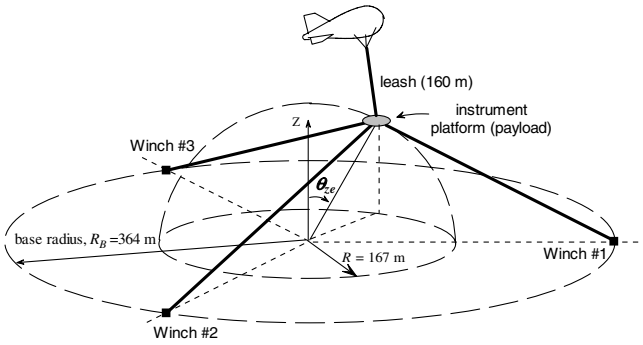

a)

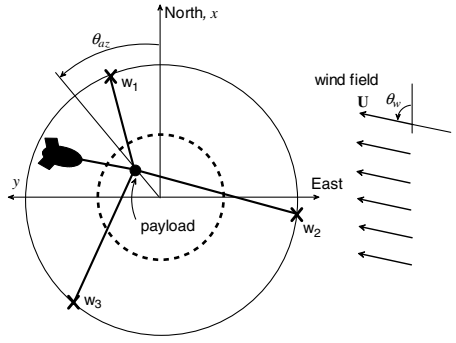

b)

Fig. 2 Experimental positioning system: a) schematic diagram and b) top view.

manipulator). Researchers in China have recently studied a cable manipulator that is at a similar scale to our system [9], which is also designed as a positioning device for a large radio telescope. The main difference with the Chinese concept is that instead of using an aerostat for lift, its receiver is suspended from multiple cables extending radially to tall tower supports. An experimental system was built [10], but no results have been published as of yet.

Astronomers in France have developed and tested a multitethered aerostat system for use with an optical telescope [11]. The architecture tested uses six support tethers arranged so that only a single winch is necessary to track an object. Astronomical observations were successful, however, only very limited quantitative results regarding the dynamic behavior of the system were presented.

The performance of a tritethered aerostat system has been studied at the theoretical level using simulations of a discretized dynamics model of the system [12,13]. The method for varying the length of the cable using a lumped-mass model is similar to a technique developed for simulating marine cables in reel-in/payout operation [14]. The initial study of the actuated multitethered system suggested that the tethers, although long (greater than 800 m), were effective in reducing the motion of the antenna payload subject to a wind disturbance [12]. To corroborate the simulation results and assess the feasibility of the positioning system, a one-third scale experimental system of the multitethered aerostat was constructed at the Dominion Radio Astronomical Observatory (DRAO) in Penticton, British Columbia, Canada [15]. Experiments were performed in the spring of 2004 and 2005. The first step of the model validation was to compare results for the system without tether actuation [16]. The dynamics model predicted the passive response of the system well, although uncertainty in measuring and approximating the actual wind field limited the ability to mimic field conditions with certainty.

In this paper, the dynamics of a tritethered aerostat system using time-varying tether lengths is investigated experimentally and our dynamics model is validated through a comparison of results with active winches under both open and closed-loop control. This work represents the first experimental model validation for a large-scale cable positioning system and the first experimental validation of the length-varying lumped-mass model for cable actuation [14].

II. Experimental System

The experimental system was sized to represent a one-third scale version of the proposed LAR telescope [15]. The four major components of the experimental system are 1) the aerostat, 2) the tethers, 3) the payload sensors or instrument platform, and 4) the winches. Photographs of the various components are presented in Fig. 3, and Table 1 summarizes the hardware characteristics.

The helium-filled aerostat, manufactured by Worldwide Aeros of California, has an internal air ballonet with fans/vents to regulate the internal pressure. The tethers are produced by Cortland Cable and are made of Plasma: a light, high-strength, high-stiffness braided rope made from ultrahigh molecular weight polyethylene. The upper tether connecting the instrument platform to the aerostat is referred to as the *leash*. It has a fixed length of 160 m and contains conductors that are used to transmit power and data to the aerostat. The instrument platform is a 0.8-m circular plate attached to the three tethers at the confluence point by Teflon-coated hangers.

The bottom of the tethers are attached to winches placed equidistant from each other on a circle of radius of 364 m. The winches actively adjust the lengths of the tethers to position the payload to various locations in the sky and to reduce low-frequency perturbations to the platform. The winches are powered by 2.8-kW servomotors produced by Bosh Rexroth through 100:1 alpha gear reducers. The entire winch swivels about a vertical axis, permitting the winch to always point toward the confluence point of the tethers. From the winch drum, the tether passes through a level wind and a fairlead to ensure that the tether wraps onto the drum in an orderly manner.

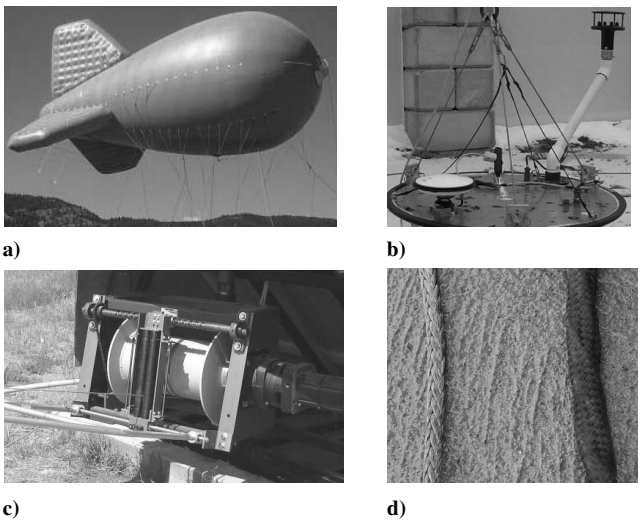

a) b) c) d)

Fig. 3 Experimental system components: a) BOB, an 18-m Worldwide Aeros aerostat, b) instrument platform, c) winch, and d) tethers.

Table 1 Characteristics of aerostat, tethers, instrumentation, and winches

Aerostat	
Diameter	7.7 m
Length	18 m
Volume	530 m^3
Max net lift	2550 N
Tethers	
Diameter	5 mm
Length	~400 m
Density	840 kg/m^3
Young's mod.	37.4 GPa

Instruments	
DGPS	Novatel, FlexPak-G2L
Load cells	Massload Tech., ML200
Wind	Gill Instruments Windsonic, 2-D
Winches	
Motor	Bosch Rexroth MHD090
Gearing	Alpha 100:1, 2-stage planetary
Extras	Level wind and fairlead

III. Control Architecture

A schematic of the PC-based control architecture is shown in Fig. 4. Three PCs are used to retrieve feedback data and send out control commands to the three winch motors connected in series. Sensor data are collected from three sources: 1) the airborne GPS receivers transmitting measurements via a radio modem, 2) the base GPS receiver using a serial cable, and 3) the load cell and wind sensors, which are digitized at a rate of 10 Hz on the platform and transmitted in a single RS-485 data stream down the central conductor. A Labview program records and displays the measured data using the GPS time stamp for synchronization. Real-time GPS processing software (RTKNav, from Waypoint Consulting) combines each signal from the aerial receivers with data from the base receiver to produce 10-Hz differential GPS position measurements. The position of the platform is sent to the feedback control software, LARCon, which computes appropriate winch commands. The commands are passed to the motor controller, Bosch's PPC, which issues speed commands to the individual motor drives. Visual Motion is Bosch's proprietary software that enables the user to specify and monitor the operation of the motors.

A block diagram of the winch control system, which operates at the 10-Hz measurement frequency, is given in Fig. 5. The experimental closed-loop testing of the positioning system used a proportional, integral, and derivative (PID) controller. The general equation for the PID controller is as follows:

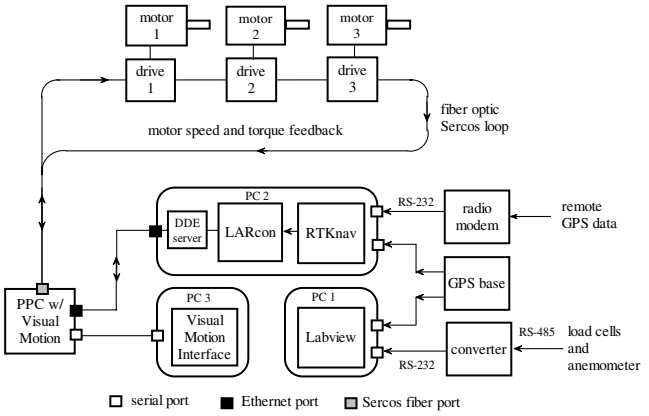

Fig. 4 Architecture for PC-based measurement and motor control system.

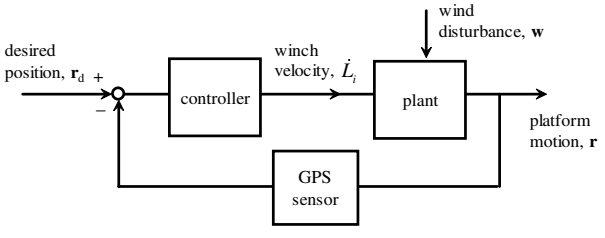

Fig. 5 Block diagram of overall winch control system.

$$\dot{L}_i = K_D \dot{e}_i + K_P e_i + K_I \int e_i \, dt \tag{1}$$

where $\dot{L}_i$ is the tether velocity for winch i, and e_i is the instantaneous error of the corresponding distance from the winch to the payload. The error is calculated using

$$e_i = ||\boldsymbol{r}_d - \boldsymbol{r}_{Wi}|| - ||\boldsymbol{r} - \boldsymbol{r}_{Wi}|| \tag{2}$$

(also see Fig. 6). The idea behind this approach is that the only payload location at which $e_i = 0$ for $i = 1, \ldots, 3$ is where $\boldsymbol{r} = \boldsymbol{r}_d$. Thus, we can rely on an individual control for each tether, acting together, to bring the payload to its desired location.

This three-degree-of-freedom (DOF) positioning system does not consider orientation, because the payload is assumed to be a single point mass. Orientation control of the receiver is important for operation of the actual LAR telescope, and it is envisioned that expanding the system to include six tethers will give the system some level of orientation control. A secondary mechanism is planned that will be attached to the receiver platform to achieve the required level of orientation control.

IV. Dynamics Model

The complete dynamics model of the system consists of the following elements: 1) a discretized cable model for the three ground tethers and the aerostat leash; 2) a feed or receiver, modeled as a simple spherical shell; 3) an aerodynamics model of a streamlined aerostat; 4) a full-field wind model, including turbulence, and 5) a simplified model of the motor/winch actuator. Details of the development of the dynamics model have been previously reported by Nahon [12,13].

The tether winching system is included in the dynamics model by actively adjusting the length of the bottommost tether element according to the desired controller input. This discrete step change to the tether length approximates the continuous length change achieved by the real winching system. Typically, the iteration time step of the simulation is 1 ms or less, which provides a smooth response and small instantaneous length changes.

A PID controller is implemented in the simulation in a manner similar to the experimental system [i.e., using Eqs. (1) and (2)]. The control input is velocity command $\dot{L}_i$, which is converted to a tether length using numerical integration. As the tether length changes, the mass of the two lowermost tether nodes also changes accordingly. This method has also been applied to towed marine systems [14], but

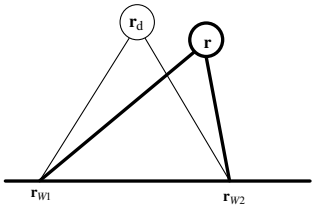

Fig. 6 Two-dimensional representation of tether geometry showing the payload's current position and desired position.

the current work represents the first time this approach has been directly compared with experimental data.

The initial model of the multitethered aerostat system [12] assumed ideal winches that could respond instantly to control commands, with the feedback loop synchronized with the simulation integration time step. The 10-Hz bandwidth of the GPS sensors is far below the integration bandwidth, which usually exceeds 1000 Hz. Therefore, the simulation was adapted to reflect this limitation by making position updates available to the controller at only 10 Hz. As in the real system, the winch velocity commands were constant in the interval between position updates. The dynamic response of the winch system to the commanded velocity is modeled as a second-order system governed by the following transfer function:

$$\frac{v_i(s)}{\dot{L}_i(s)} = \frac{\omega_n^2}{s^2 + 2\zeta\omega_n s + \omega_n^2} \tag{3}$$

where v_i is the output velocity of the winch and $\dot{L}_i$ is the commanded velocity. The damping ratio $\zeta = 0.44$ and natural frequency $\omega_n = 200$ rad/s were estimated from experimental step response tests performed on individual winches [17].

V. Results

As mentioned in Sec. I, the first stage of validating the dynamics model, complete with the aerostat model, was based on passive tethers [16]. The model gave encouraging results, however, there was some imprecision due to uncertainty with recreating the precise wind input. To validate the model of the dynamic actuation of the tethered system against the experimental system, it was decided to remove as much of the wind uncertainty as possible. This was achieved by first analyzing the response of the complete system to open-loop control inputs in calm conditions. This was then followed by an analysis of the closed-loop response of the system in a variety of wind conditions, but with the aerostat aerodynamics represented in the simulation by a measured leash force.

A. Open Loop

A direct approach to assess the winch and tether model is to compare its open-loop response with that of the experimental system. The platform position in response to open-loop sinusoidal winch inputs was measured on four separate flights. Each flight was conducted in the early morning to ensure wind disturbances would be minimal (the measured wind speed at the platform was less than 1 m/s).

To compare results, the dynamics model was linearized using numerical techniques [17] and its corresponding Bode diagram for magnitude and phase was directly compared with the Bode plots obtained from flight data. Figure 7 gives separate Bode plots for each of the three Cartesian coordinates of the inertial frame. The input to the system is a sinusoidal length change in tether 1 and the system is in the symmetric configuration (i.e., $\theta_{ze} = 0$ deg). Because of acceleration limits of the winch motors, the highest frequency tested was 2.5 Hz. For the high-frequency tests, particularly in the z direction, it was not possible to estimate the phase angle satisfactorily, because the motion had a small magnitude and was corrupted by noise.

The results in Fig. 7 show a good match between the linear model and the measured frequency response. The general shape and main features of the Bode plot are present in both sets of results. The main peak of the linear model for the magnitude of the x and y horizontal directions may be shifted slightly toward lower frequencies, but it appears to have the appropriate magnitude.

In the vertical direction, there is good agreement at low frequencies, but the results diverge at higher frequencies. For most of the divergence region, the magnitudes are quite low, and so the discrepancy could be attributed to insufficient measurement resolution. However, even if it is a real discrepancy in the model, the magnitude is low enough that it will have a minimal impact on the results. The exception is the peak at 2 Hz, which crosses the 0-dB line. The response at this frequency appears to be overstated in the model, and as a result, the vertical motion in the simulation may have a larger amplitude at this frequency. The lower-frequency region of the Bode plots is far more critical when assessing the quality of the simulation, because the bulk of the input forces are low frequency due to the substantial size of the system (i.e., the first longitudinal and transverse natural frequencies of an individual tether are <0.5 Hz).

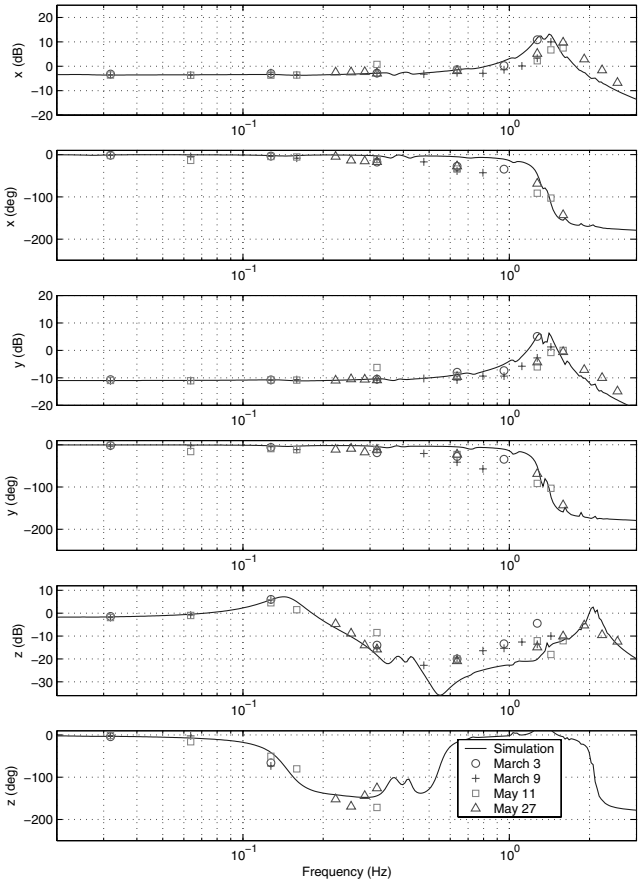

Fig. 7 Bode plot comparison of simulated and experimental payload position in response to input at winch 1.

During the test flights, the peak in the vertical magnitude at 0.15 Hz has been observed to dominate the overall motion of the platform. When the system operated in closed loop, this vertical *bounce* mode was the first to become unstable with high control gains. Based upon test data near the frequency of this mode, it appears to be characterized well by the simulation. A modal analysis for this mode suggests that its stability can be improved by decreasing the stiffness of the aerostat's leash [17].

B. Closed Loop

The nonlinear model of the feedback control system, including the winch actuators, can be validated by comparing simulation and experimental output with matching disturbances. This procedure assumes that the majority of the disturbances are generated by the aerodynamic forces on the aerostat and transmitted to the platform through the leash, which has been confirmed [18]. The leash tension was measured during the flight tests and it can be expressed in Cartesian components by assuming its direction is coincident with the relative position vector between the aerostat and the platform, as measured by GPS. This Cartesian force is added to the simulation by removing the aerostat aerodynamics and applying the measured leash force to the uppermost leash node. Although this removes the aerostat's dynamic response to specific control inputs, the motion associated with the control input is very small compared with the original aerostat motion (centimeters compared with tens of meters) imbedded in the measured leash tension. Wind-induced forces on the

tethers and the platform are included in the simulation results, but these forces are relatively inconsequential compared with the much larger leash force.

The results from two specific flights will be used to demonstrate the merits of the dynamics model and the effectiveness of the actual control system. The first flight occurred on 6 May 2005 and was at a zenith angle near zero, hence, with a symmetrical tether arrangement. The second flight, on 27 May 2005, was with an asymmetrical tether arrangement at a zenith angle of 50 deg, which is near the 60-deg operational limit of the LAR telescope. The azimuth angle for the high zenith case was −38 deg, which is known to be among the most poorly behaved locations in the workspace. The gains for the PID controller were tuned at the start of each test using trial and error. Our simulation has been used in the past to select optimized PID gains [14], but because of sensor noise and other unmodeled effects associated with the experimental system, lower gains were required in practice, to achieve stability. If the gains were tuned too aggressively ($K_P > 0.5$), the vertical mode near 0.15 Hz often became unstable.

During each flight, two separate trials were performed: the first with the feedback control activated and the second with no control (fixed tether lengths). The experimental results for each trial are presented, along with two sets of simulation result: one with the same control scheme tested during that trial and one with the opposite control scheme (i.e., if a controller was tested, the opposite control scheme is with no controller and for the tests without control, the opposite scheme is with control). With matching control, a comparison of the simulated/experimental results appraises the accuracy of the model predictions, whereas the results with the opposite control scheme provide an estimation of the effectiveness of the actual control system. For the experiments with control, the simulated results without control provide a benchmark to quantify how much improvement can be attributed to the controller. For the experiments without control, the simulated results with control provide a prediction of how much the controller might have changed the results had it been active. The reliability of this controller evaluation depends on the quality of the simulation, which will be demonstrated using the first set of simulation results.

The results for the four trials are summarized in Tables 2 and 3 and plotted in Figs. 8–11. The tables include the standard deviation of the platform position and the mean and standard deviation of the tether tension. Only tensions in tethers 1 and 3 are reported, because the load cell for tether 2 malfunctioned during the tests. The x, y, and z positions of the platform are plotted against time and the power spectral density (PSD) of the position in the x and z directions are included in the figures (the PSD of y was omitted, because it strongly resembles the PSD of x). The general effectiveness of the controller is demonstrated by the reduced standard deviations for the experimental platform position during trials 1 and 3 compared with their respective uncontrolled counterparts.

The simulation results with the matching control schemes correspond closely to the experiments for all four trials, but the agreement is clearly better for trials 1 and 2 with the system in the zenith configuration. There is substantial noise with the GPS measurements, which is most noticeable in the x direction of Fig. 8 for trial 1, in which the motion was small. The presence of noise is also apparent in all the experimental PSD plots as a flattening of the curves at high frequencies. Despite the measurement noise, it is observed that the simulation clearly predicts the low-frequency motion accurately, which can be seen in both the time histories and the PSD plots. It should be noted that any difference in the mean value of the positions is not significant, because it is due to inexact initial conditions. The simulation starts from a static equilibrium position, whereas at $t = 0$ of the measurements, the actual system has dynamic motion.

For trial 1, the standard deviation of the simulated vertical motion is within 5 mm of the measured motion and the difference between the horizontal deviations is less than 1 mm. For trial 2, the system is uncontrolled and the difference between the simulation and experiment is 14 mm vertically and less than 5 mm horizontally. Considering the scale of the system, the accuracy of simulation with and without the feedback control system strongly validates the tether and winch models.

During trial 2, a horizontal oscillation at 0.2 Hz was measured that cannot be attributed to sensor noise. The oscillation does not show up in the simulation results, which can be seen toward the end of the time histories and in the horizontal PSD, with the missing peak at 0.2 Hz. It is difficult to ascertain what is causing the oscillation, but it does not appear to originate from the disturbance force transmitted through the leash. The slack central tether used during deployment and retrieval, which is attached to the tether confluence point, is not included in our dynamics model and it is possible that it can have a

Table 2 Comparison of experimental and simulated results at the zenith with and without control for tests on 6 May 2005. The PID gains used were $K_p = 0.3\ \mathrm{s}^{-1}$, $K_d = 0.05$, and $K_i = 0.05\ \mathrm{s}^{-2}$

		Trial 1, mean wind = 1.2 m/s			Trial 2, mean wind = 0.88 m/s		
Control		Yes	Yes	No	No	No	Yes
Type		Exp.	Sim.	Sim.	Exp.	Sim.	Sim.
Platform	σ_x	0.0018	0.0012	0.0028	0.0049	0.0045	0.0015
Position, m	σ_y	0.0034	0.0036	0.0107	0.0117	0.0135	0.0042
	σ_z	0.022	0.027	0.054	0.053	0.067	0.026
	T_1	1495	1415	1415	1489	1424	1424
Tether	σ_{T1}	36	37	37	47	48	48
Tension, N	T_3	1312	1328	1328	1296	1300	1299
	σ_{T3}	36	37	36	49	52	52

Table 3 Comparison of experimental and simulated results at extreme zenith angle with and without control for tests on 27 May 2005. The PID gains used were $K_p = 0.4\ \mathrm{s}^{-1}$ and $K_d = K_i = 0$.

		Trial 3, mean wind = 4.0 m/s			Trial 4, mean wind = 3.8 m/s		
Control		Yes	Yes	No	No	No	Yes
Type		Exp.	Sim.	Sim.	Exp.	Sim.	Sim.
Platform	σ_x	0.056	0.043	0.082	0.073	0.072	0.036
Position, m	σ_y	0.046	0.036	0.077	0.064	0.065	0.030
	σ_z	0.092	0.107	0.215	0.156	0.184	0.084
	T_1	2160	2170	2171	2241	2264	2262
Tether	σ_{T1}	136	141	138	112	117	119
Tension, N	T_3	492	529	531	516	538	536
	σ_{T3}	55	54	52	42	44	46

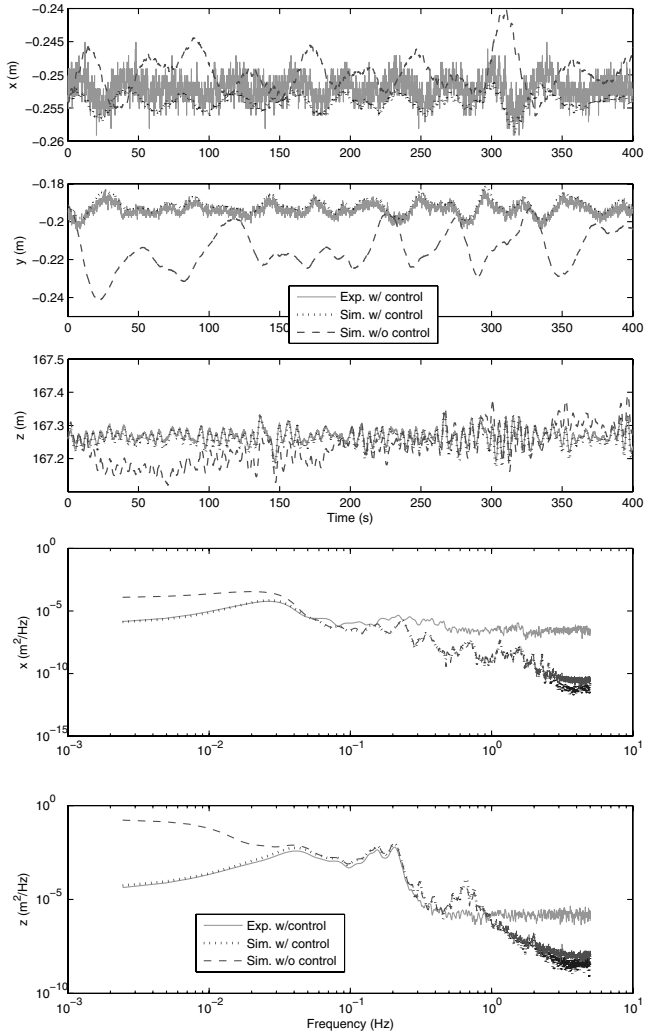

Fig. 8 Comparison of time history and PSD of experimental and simulated position for trial 1 (test near zenith with control). The simulated response without control is also given.

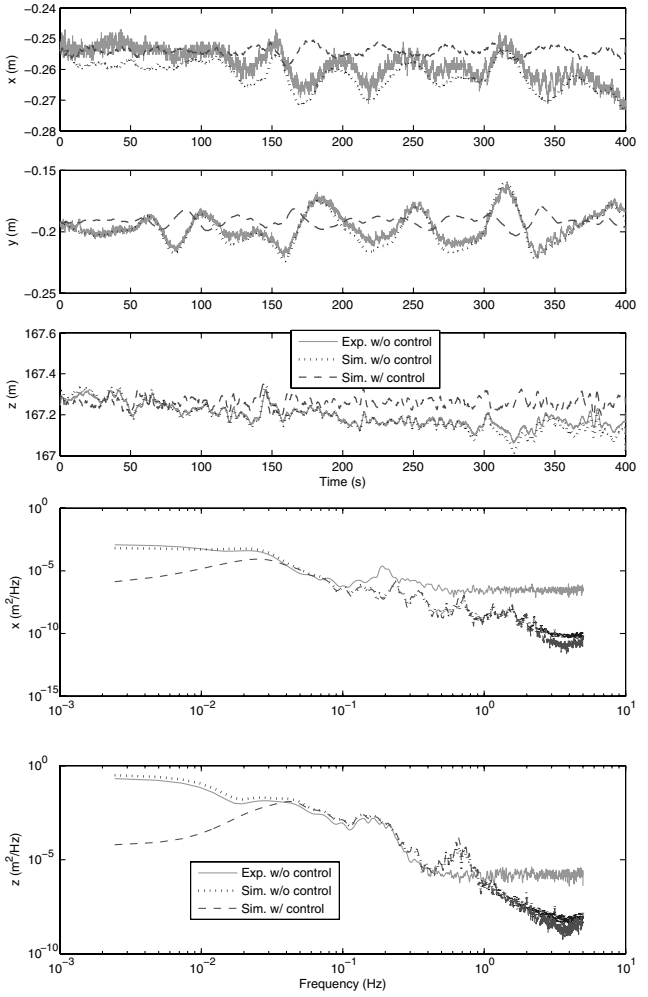

Fig. 9 Comparison of time history and PSD of experimental and simulated position for trial 2 (test near zenith without control). The simulated response with control is also given.

small impact on the platform motion. The simulated results for trials 1 and 2 show a peak in the vertical PSD plot near 0.7 Hz that is not present in the measurements. Overall, the magnitudes of the inconsistent oscillations in the simulation are relatively small (about 1 cm), and because the simulation accurately predicts the higher-amplitude low-frequency motion, the results are deemed satisfactory.

The simulation results at a high zenith angle, trials 3 and 4 in Figs. 10 and 11, do not match the measurements as well as at the previous trial at the zenith. The general characteristics of the motion are predicted well, as observed by the similarity in the PSD plots, but the amplitude of the oscillations are not always accurate, which is observed in the time histories and the statistics in Table 3. One explanation for degraded accuracy of the simulation at high zenith angles is that in this configuration, the system is less stiff and therefore more sensitive to estimation errors. The system loses stiffness as the three tethers become asymmetric, because the tension in at least one tether inevitably drops. For the configuration tested in trials 3 and 4, the tension in tether 3 drops substantially below the other two. The stiffness of an individual tether depends greatly on its tensile load, because the amount of sag in the tether profile drastically affects its stiffness. Therefore, at the high zenith angle configuration, any errors in the tension distribution among the tethers in the model will result in greater discrepancies than for the symmetric case at the zenith. This is confirmed by the results of trials 1 and 2, because the simulated mean tether tensions differed from the measured tensions by larger amounts than in trials 3 and 4, although still producing excellent agreement in the motion. Although the mean tensions have a dc error, the standard deviation of the tensions are similar, indicating that the disturbing functions were similar.

The imprecision in the model's distribution of forces to the three support tethers could be caused by assuming that all three tethers and the leash meet at a single point mass or node at the confluence point. The entire platform weight and the associated weight of the slack central tether are applied to this node, whereas in the real system, the weight of the platform and the central leash are likely to be distributed unequally between the three tethers. Despite the discrepancy in mean tether loading and its implications at the high zenith angle, the simulation is proven effective at predicting the response of the system with and without a controller.

With the first set of simulation results verifying the reliability of the model, the second set of simulation results can be used to evaluate the effectiveness of the controller. This approach is more direct than comparing the two separate time histories of the motion that were exposed inevitably to different wind disturbances. The dashed-dotted lines in Figs. 8–11 show the predicted response of the system if the opposite control scheme would have been used. It is clear that the controller is very effective at limiting low-frequency motion in all three directions, and in terms of its standard deviation, in all four trials, the controller reduces the motion in all three directions by roughly 50%.

Improved performance can be achieved in the simulation by using higher gains, namely, proportional and derivative. However, during the test flights, instabilities occurred if the gains were increased beyond the values given in Tables 2 and 3. The experimental gains are limited by GPS measurement noise, which is not included in the model. From the PSD plots, it is observed that the controller is most

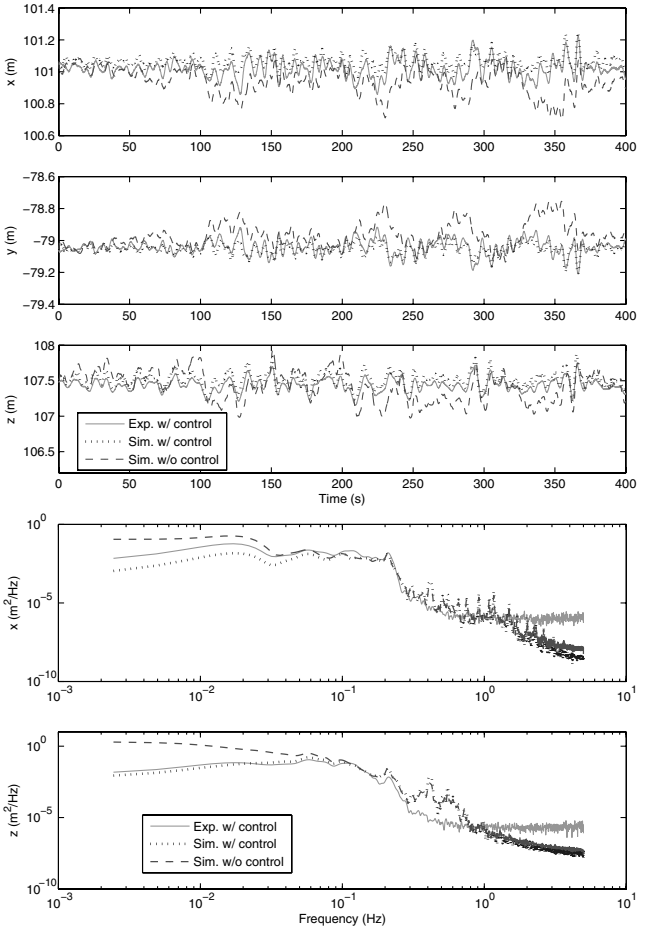

Fig. 10 Comparison of time history and PSD of experimental and simulated position for trial 3 (test at $\theta_{ze} = 50\,\mathrm{deg}$ with control). The simulated response without control is also given.

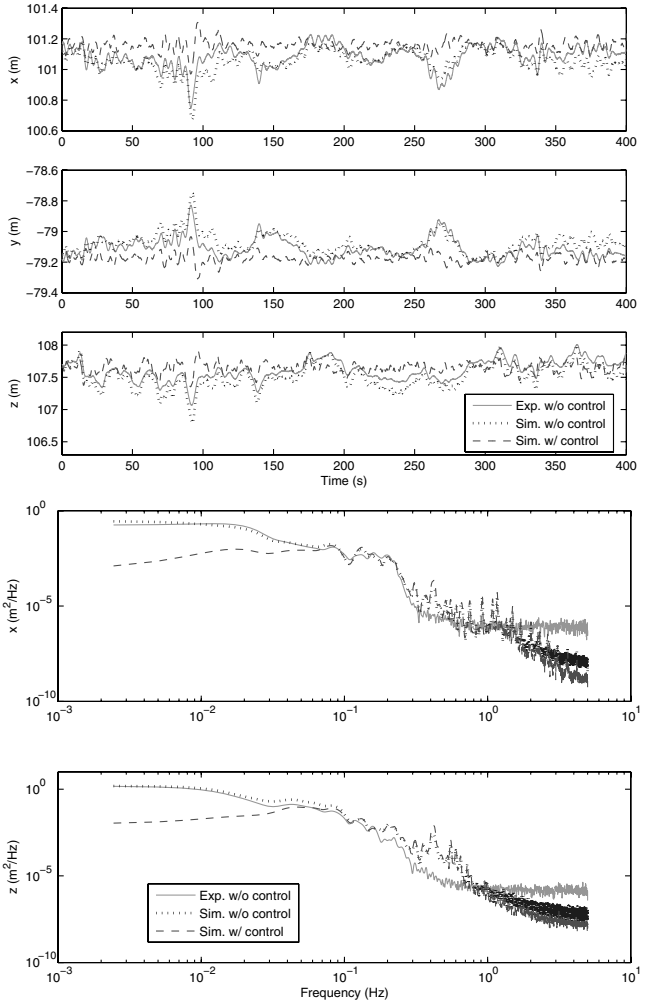

Fig. 11 Comparison of time history and PSD of experimental and simulated position for trial 4 (test at $\theta_{ze} = 50\,\mathrm{deg}$ without control). The simulated response with control is also given.

effective at the lowest frequencies, and beyond about 0.05 Hz, the controller has little impact. Future efforts will focus on expanding its effective bandwidth with the use of more advanced controllers than the simple PID controller used thus far. The dynamics model will be a useful tool for designing and evaluating controllers before implementation on the experimental system.

VI. Design Application

With the dependability of the dynamics model established, it becomes a valuable design tool to evaluate and compare modifications to the positioning system. To illustrate this, the behavior of the system is evaluated after changing two important design parameters: the number of support tethers and the size of the winch perimeter or base radius. Increasing the number of tethers beyond three potentially improves the positioning system, because the additional tethers have the ability to stiffen the structure by maintaining tension during highly asymmetric configurations at extreme zenith angles. On the other hand, adding tethers also adds weight to the system, which reduces the amount of aerostat buoyancy that serves to tension the system. To analyze the precise implications of using more tethers, simulations were performed using 3, 4, 5, and 6 tethers.

Simulation results are presented for two configurations: the symmetric case at the zenith and at the maximum zenith angle of 60 deg. The leash disturbance force implemented in the simulation was taken from trial 3 on 27 May because of high winds during that test. A base radius of $R_B = 400$ m was used, which is greater than the experimental base radius of 364 m (at 364 m, it was not possible to reach a zenith angle of 60 deg). A proportional controller with a gain of 0.4 was used for all simulations in this section to correspond with the practical gains used during the experiments. The results are summarized in Table 4, which gives the standard deviation or root mean square (rms) of the position error. The error presented is separated into the error in the focal plane and out of the focal plane of the proposed radio telescope. The focal plane is tangent to the hemisphere of desired platform locations, and the error in this plane is of primary importance for telescope operation.

At the zenith, there is an insignificant difference between the results, although the six-tether case has the largest errors. This suggests that at the zenith, the additional weight from the three extra tethers impedes performance more than their added stiffness improves it. For the $\theta_{ze} = 60\,\mathrm{deg}$ case, the opposite is true, because

Table 4 Comparison of simulated results with different numbers of tethers for cases with a base radius of 400 m.

Zenith angle, θ_{ze}	0				60			
No. of tethers	3	4	5	6	3	4	5	6
RMS error in focal point	0.002	0.002	0.002	0.002	0.070	0.045	0.038	0.036
RMS error out of focal point	0.028	0.027	0.028	0.033	0.041	0.034	0.031	0.032

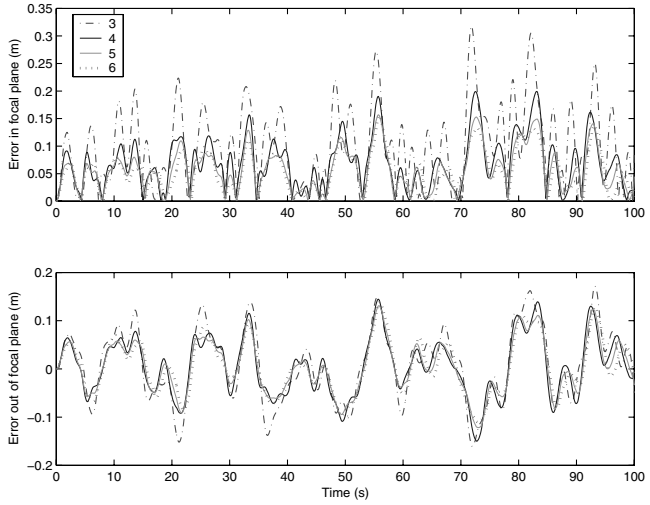

Fig. 12 Comparison of simulated position error for the system at $\theta_{ze} = 60$ deg with 3, 4, 5, and 6 tethers.

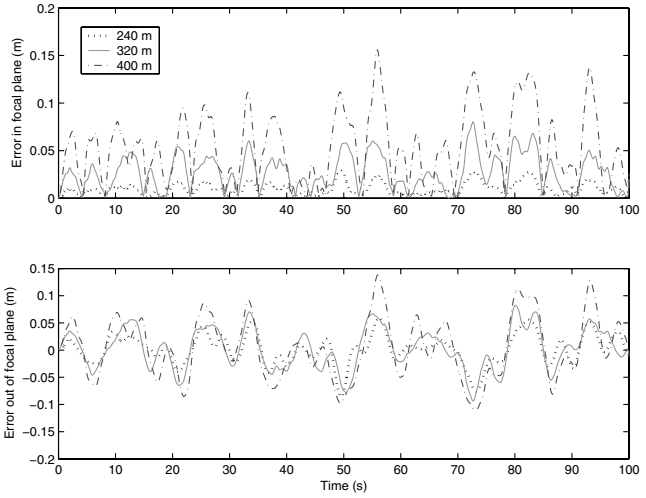

Fig. 13 Comparison of simulated position error for the system at $\theta_{ze} = 60$ deg with six tethers and a base radius ranging from 240 to 400 m.

the position error is clearly reduced as the number of tethers increases, with the best performance in the focal plane achieved with six tethers. A plot of the results for the high zenith angles is given in Fig. 12.

To fully take advantage of using more than three tethers, it is helpful to reduce the base radius, which reduces tether weight and hence increases tension. It is only possible to reduce the base radius by adding extra tethers to provide the geometric configuration necessary at high zenith angles. To study the effect of reducing the base radius, further simulations were performed with six tethers at base radii of 320 and 240 m. The results for both zenith angles are summarized in Table 5, and the $\theta_{ze} = 60$ deg case is plotted in Fig. 13. At the zenith, reducing the base radius has little effect in the focal plane, but out of the focal plane, the error decreases. This is not surprising, because at the zenith, out of the focal plane corresponds to the vertical direction and as the base radius shrinks, the tethers become more vertical and hence stiffer in the vertical direction. At $\theta_{ze} = 60$ deg, the improvement in the focal plane is significant, because the mean error is reduced from 5 to 1 cm.

Coupling the improvement from increasing to six tethers and reducing the base radius to 240 m, the rms error in the focal plane at $\theta_{ze} = 60$ deg improved by an order of magnitude from 70 to 7 mm. Based on these results, six tethers with a base radius of 240 m appears to be the most logical choice for the design of the telescope. The actual telescope will have a substantial feed or antenna structure located at the platform, and using six tethers also enables the system to achieve some level of orientation control of the feed.

VII. Conclusions

A tritethered aerostat positioning system for a large-scale radio telescope using feedback control was tested at one-third scale. The flight test results suggest that the control system is able to reduce payload motion approximately in half, while subject to wind disturbances. A dynamics model based on discretized tethers and a second-order winch system was demonstrated to accurately predict the experimental system. The open-loop frequency response of platform motion to winch inputs compared favorably to Bode plots of the linearized model. Next, the nonlinear model was subject to the actual measured disturbances and the time histories and spectral densities of the platform motion during both closed-loop and uncontrolled scenarios were shown to agree well with the measurements. Two cases were studied representing the nominal zenith symmetric configuration and a high zenith configuration, and the simulation was observed to be less accurate at the high zenith angle. The stiffness of the system is much more sensitive to discrepancies in tether loads at high zenith angles, because at least one tether is in low tension. As a result, the tether will sag, and even a small discrepancy in the tension distribution in the model will cause the simulated platform position to be noticeably less accurate. Despite the increased sensitivity at high zenith angles, the standard deviation of the simulated position of the platform with active control differed by as little as 15 mm from the measured position. This level of accuracy is encouraging when the scale of the overall system is considered.

To demonstrate the utility of the validated model as a design tool, the number of support tethers and the size of the winch perimeter were varied while the performance of the system was investigated. It was shown that at the zenith, adding more tethers does not appreciably improve performance, but at the extreme zenith angle, using six tethers and a reduced winch perimeter radius reduced the mean error by an order of magnitude relative to using three tethers. As the LAR radio telescope design advances, the model will be an important tool in fine-tuning important design variables and controllers.

References

[1] Fitzsimmons, J. T., Veidt, B., and Dewdney, P., "Steady-State Analysis of the Multi-Tethered Aerostat Platform for the Large Adaptive Reflector Telescope," *Proceedings of the Society of Photo-Optical Instrumentation Engineers (SPIE)*, Vol. 4015, International Society for Optical Engineering, Bellingham, WA, 2000, pp. 476–487.

[2] Leclaire, R. C., and Rice. C. B., "The Local Motions of a Payload Supported by a Tritethered Natural Shape Balloon," U.S. Air Force, Rept. AFCRL-TR-73-0748, 1973.

[3] Masterskikh. M. A., "A Method for Holding a Pilot Balloon or Light Aerostat at a Predetermined Height for Meteorological Observations," *Meteorologiya i Gidrologiya*, No. 4, 1978, pp. 102–104.

[4] Albus, J., Bostelman, R., and Dagalakis, N., "The NIST Robocrane," *Journal of Robotic Systems*, Vol. 10, No. 5, 1993, pp. 709–724.

Table 5 Comparison of simulated results for cases with six tethers and base radii ranging from 240 to 400 m.

Zenith angle, θ_{ze}	0			60		
Winch radius	240	320	400	240	320	400
RMS error in focal point	0.002	0.003	0.002	0.007	0.018	0.036
RMS error out of focal point	0.009	0.017	0.033	0.018	0.021	0.032

[5] Roberts, R., Graham, T., and Lippit, T., "On the Inverse Kinematics, Statics, and Fault Tolerance of Cable Suspended Robots," *Journal of Robotic Systems*, Vol. 15, No. 10, 1998, pp. 581–597.

[6] Kossowski, C., and Notash, L., "Cat4 (Cable Actuated Truss, 4 Degrees of Freedom): A Novel 4 DOF Cable Actuated Parallel Manipulator," *Journal of Robotic Systems*, Vol. 19, No. 12, 2002, pp. 605–615.

[7] Barrette, G., and Gosselin, C., "Determination of the Dynamic Workspace of Cable-Driven Planar Parallel Mechanisms," *Journal of Mechanical Design*, Vol. 127, No. 2, 2005, pp. 242–248.

[8] Pusey, J., Fattah, A., Agrawal, S., and Messina, E., "Design and Workspace Analysis of a 6-6 Cable-Suspended Parallel Robot," *Mechanism and Machine Theory*, Vol. 39, No. 7, 2004, pp. 761–778.

[9] Duan, B., "A New Design Project for the Lin Feed Structure for Large Spherical Radio Telescope and its Nonlinear Dynamics Analysis," *Mechatronics*, Vol. 9, No. 1, 1999, pp. 53–64.

[10] Qiu, Y., Sheng, Y., and Duan, B., "Indirect Calibration of Initial Cable Lengths of a Huge Parallel Cable Robot," *Chinese Journal of Mechanical Engineering*, English ed., 2004, pp. 79–81.

[11] Le Coroller, H., Dejonghe1, J., Arpesella C., Vernet, D., and Labeyrie, A., "Tests with a Carlina-Type Hypertelescope Prototype," *Astronomy and Astrophysics*, Vol. 426, No. 2, 2004, pp. 721–728.

[12] Nahon, M., "Dynamics and Control of a Novel Radio Telescope Antenna," *Proceedings of the AIAA Modeling and Simulation Technologies Conference*, AIAA, Reston, VA, 1999, pp. 214–222.

[13] Nahon, M., Gilardi, G., and Lambert, C., "Dynamics and Control of a Radio Telescope Receiver Supported by a Tethered Aerostat," *Journal of Guidance, Control, and Dynamics*, Vol. 25, No. 6, 2002, pp. 1107–1115.

[14] Kamman, J. W., and Huston, R. L., "Modeling of Variable Length Towed and Tethered Cable Systems," *Journal of Guidance, Control, and Dynamics*, Vol. 22, No. 4, 1999, pp. 602–608.

[15] Lambert, C., Saunders, A., Crawford, C., and Nahon, M., "Design of a One-Third Scale Multi-Tethered Aerostat System for Precise Positioning of a Radio Telescope Receiver," *Proceedings of the Canadian Aeronautics and Space Institute (CASI) Annual General Meeting and Conference* [CD-ROM], Canadian Aeronautics and Space Institute, Ottawa, Ontario, Canada, 2003.

[16] Lambert, C., Nahon, M., and Chalmers, D., "Study of a Multi-Tethered Aerostat System: Experimental Observations and Model Validation," *Proceedings of the 16th AIAA Lighter-than-Air Systems Technology Conference*, 2005.

[17] Lambert, C., "Dynamics and Control of a Multi-Tethered Aerostat Positioning System," Ph.D. Thesis, McGill Univ., Montreal, Quebec, Canada, 2006.

[18] Deschesnes, F., and Nahon, M., "Design Improvements for a Multi-Tethered Aerostat System," *A Collection of Technical Papers: AIAA Atmospheric Flight Mechanics Conference*, AIAA, Reston, VA, 2005, pp. 994–1005; also AIAA Paper 2005-6126.